

Irreversibility of decorrelating processes: an experimental assessment in cavity QED

Guillaume Cœuret Cauquil,^{1,2} Patrice A. Camati,³ Irénée Frerot,^{3,4}
Zheng Tan,^{1,*} Alexia Auffèves,^{3,5,6} and Igor Dotsenko^{1,2,†}

¹*Laboratoire Kastler Brossel, Collège de France, CNRS, ENS-Université PSL, Sorbonne Université, 11 place Marcelin Berthelot, 75005 Paris, France*

²*Laboratoire Collisions Agregats Rèactivité, CNRS, Université de Toulouse, 118 route de Narbonne, 31062 Toulouse, France*

³*Université Grenoble Alpes, CNRS, Grenoble INP, Institut Néel, 38000 Grenoble, France*

⁴*Laboratoire Kastler Brossel, Collège de France, CNRS, ENS-Université PSL, Sorbonne Université, 4 place Jussieu, 75005 Paris, France*

⁵*MajuLab, CNRS-UCA-SU-NUS-NTU International Joint Research Laboratory*

⁶*Centre for Quantum Technologies, National University of Singapore, 117543 Singapore, Singapore*

Entropy production quantifies the amount of irreversibility of a physical process, leading to fundamental bounds for thermodynamic quantities. Particularly in the quantum realm, considerable research has been carried out in the last decades extending entropy production to nonequilibrium processes. We experimentally investigate the entropy production of forward-backward cycles containing different decorrelating processes realized to erase different types of correlations between two interacting systems, from obliterating solely quantum coherence to completely decorrelating local states. We apply these processes to the entanglement of a two-level atom, realized with a circular Rydberg atom, and a light field of a high-quality microwave cavity. The entropy production is computed from the full quantum-state tomography of the system performed at different stages of the interaction-decorrelation sequence. Due to the quantum nature of the atom-cavity system, we find that, although standard, the maximum likelihood estimation method for the density matrix leads to spurious divergences of the entropy production. We propose and implement an alternative estimator that remedies such divergences. Our work experimentally assesses irreversibility of non-thermal processes and addresses the care that must be taken in handling experimental data to estimate the entropy production.

I. INTRODUCTION

The second law of thermodynamics plays a fundamental role in physics establishing the notion of irreversibility and providing constraints on the conversion of heat into work. For thermodynamically open systems, the second law is expressed as the positivity of entropy production [1], the quantifier of irreversibility. The irreversibility of a physical process can be understood as the inability to bring the system back to its initial state investing exactly the same resources that were spent in the original process. For example, consider a forward process in which the amount of work W has been extracted from a thermodynamic system that undergoes a transformation from state A to state B while absorbing the heat Q from the environment. This transformation is reversible if and only if there exists a backward process that performs the work $-W$ bringing the system back from B to A while ejecting the heat $-Q$. According to this notion, irreversibility is related to the cost of closing the forward-backward cycle.

In the last decades, considerable progress has been achieved in formally extending the concept of entropy production to microscopic nonequilibrium systems in

both the classical [2–4] and quantum [5–7] realms. In particular, an influential approach that stimulated a lot of research is the two-point measurement (TPM) scheme in stochastic quantum thermodynamics [8, 9]. In this approach, irreversibility is also associated with closing a forward-backward cycle, but the cycle is modeled with three consecutive processes: The first forward and the last backward processes are unitary, U_τ and \tilde{U}_τ , and hence reversible, while the second process, \mathcal{E} , is irreversible. The quantum trajectories given by the measured initial and final quantum states, ρ_0 and $\tilde{\rho}_\tau$, respectively, are employed to compute the entropy production of the intermediate irreversible process, see Fig. 1.

Mathematically, the entropy production takes the form of the Kullback-Leibler-Umegaki (KLU) divergence

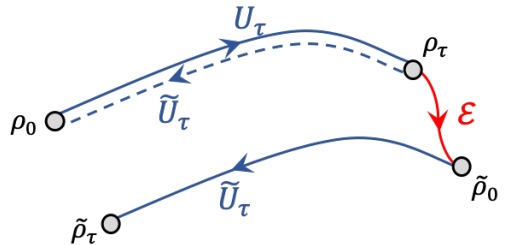


Figure 1. Forward-backward cycle in the presence of an irreversible intermediate process \mathcal{E} . In the absence of \mathcal{E} , the cycle is completely reversed (dash backward evolution).

* Present address: Innovation Academy for Precision Measurement Science and Technology, The Chinese Academy of Sciences, West No. 30 Xiao Hong Shan, Wuhan 430071, China.

† Contact author: igor.dotsenko@irsamc.ups-tlse.fr

$D(\rho_1||\rho_2)$, a common information-theoretic quantifier of the relative distance between two states, ρ_1 and ρ_2 [10, 11]. It is defined as $D(\rho_1||\rho_2) = -\text{Tr}[\rho_1 \ln \rho_2] - S(\rho_1)$, with $S(\rho_1)$ being the von Neumann entropy of state ρ_1 . The divergence D , as the entropy S , is not associated with any observable. It is a nonlinear function of the states, rendering intricate an experimental assessment of the entropy production. Nonetheless, the entropy production has been experimentally deduced not only for the typical thermodynamic process of thermalization [12–14], but also for genuinely quantum processes such as quantum measurement [15–17]. In this paper, we experimentally assess the entropy production of several different irreversible processes that erase partially or completely the correlations of a bipartite system [5].

Entanglement, or, more generally, quantum correlations [18], has been shown to be a major resource for a plethora of information processing tasks [19, 20]. However, it is very fragile and easily degraded by ubiquitous processes such as decoherence and relaxation of the constituting quantum systems. We focus on three distinct decorrelating processes that can act on a bipartite quantum system: decoherence, complete decorrelation, and local thermalization. The decoherence process completely eliminates the coherence of either one or both subsystems in their eigenbasis. This process erases all quantum correlations, but retains classical correlations between the two systems. Complete decorrelation erases all correlations, classical and quantum, that might be present in the bipartite state, leaving the reduced states intact. Local thermalization brings one of the subsystems to a thermal state, which also completely eliminates all correlations in the process. For these typical wide-spread irreversible processes, entropy production has been shown to quantify the entropic cost of erasing the corresponding correlations [5]. For the local thermalization process, the entropy production further accounts for the irreversibility of changing the reduced state to a thermal state.

We study entropy production in a test bipartite system composed of a two-level atom (circular Rydberg) resonantly coupled to the electromagnetic field of a microwave cavity (high-quality superconducting) [21]. In order to assess the entropy production, we have to experimentally estimate quantum states at reference points of a realized cycle. A typical reconstruction method is based on the maximum likelihood estimation (MLE) of quantum states from measured data. Unfortunately, a state maximizing the data likelihood may not have full support on the Hilbert space, the feature of the MLE that is usually innocuous and therefore ignored. However, a reference state of reduced support used for computing the divergence may lead to potential spurious nonphysical divergences, preventing us from adequately calculating entropy. To avoid this issue, we adapt the MLE protocol proposed in Ref. [22] and obtain more realistic full-rank density operators estimating quantum states in the cycle.

We present our results in the following way. We re-

visit the theory for obtaining the entropy production in the considered decorrelating irreversible processes via the TPM scheme in Sec. II. Section III presents the experimental setup adapted to simulate the action of different types of environment upon a quantum bipartite system. The methodology and experimental details to assess and estimate the entropy production are introduced in Sec. IV. Experimental simulation of irreversible processes along with the reconstructed system's states at different phases are presented in Sec. III. Finally, we conclude our work in Sec. VI.

II. TWO-POINT MEASUREMENT

Entropy production quantifies the amount of irreversibility of a physical process. Employing TPM schemes [5, 23], a number of fluctuation relations [24–26] for thermodynamic stochastic variables have been derived for a variety of physical processes. The underlying physical protocol considered in such methods can be decomposed into three distinct processes: a unitary forward process U , an intermediate (irreversible) process \mathcal{E} , and a unitary backward process \tilde{U} , as schematically shown in Fig. 1. In the following, we recapitulate the main ingredients of the TPM scheme and apply it to the decorrelating processes we considered.

After the forward, and reversible, process is realized, the system evolves according to an uncontrollable dynamics represented by the CPTP map \mathcal{E} , bringing the state ρ_τ to a new state $\tilde{\rho}_0 = \mathcal{E}(\rho_\tau)$. The lack of control over this intermediate process means that the suitable reverse evolution of the controllable forward process will not be capable of bringing the system back to its original state ρ_0 . Such an inability stems from the irreversibility of the intermediate process. Therefore, it is during this intermediate irreversible process that the entropy production arises. Typically, this process is taken to be a complete thermalization, leading to well-established results. However, other types of irreversible processes can be considered, like decorrelating processes erasing completely or partially the correlations in a bipartite system [5]. We come back to this class of processes shortly.

After the irreversible intermediate stage, the backward process attempts to bring the system back to its initial state, *i.e.* the initial state ρ_0 of the forward process. The backward evolution is performed via the controllable Hamiltonian $H_B(t) = H_F(\tau - t)$ bringing the initial backward state $\tilde{\rho}_0$ to $\tilde{\rho}_\tau = \tilde{U}_{\tau,0}\tilde{\rho}_0\tilde{U}_{\tau,0}^\dagger$, where $\tilde{U}_{\tau,0} = \mathcal{T} \exp \left\{ -\frac{i}{\hbar} \int_0^\tau dt H_B(t) \right\}$. We note that $\tilde{U}_{\tau,0} = U_{\tau,0}^\dagger$ [27]. Since, being fully controllable, the backward process is also reversible, and it does not carry any entropy production either.

In the TPM scheme, a measurement is performed at the beginning and at the end of the forward and backward processes. Each pair of measurement outcomes defines a forward and a backward trajectory, respectively.

The entropy production $\langle \Sigma \rangle$ of the intermediate process is obtained by appropriately averaging the ratio of forward and backward trajectory probability. The resulting entropy production ends up being given by the KLU divergence:

$$\langle \Sigma \rangle = D(\rho_\tau \parallel \tilde{\rho}_0) = D(\rho_0 \parallel \tilde{\rho}_\tau). \quad (1)$$

The first equality states that the entropy production in the irreversible process is given by the divergence between the initial and final states of this process. Similarly, since the forward and backward processes are reversible, *i.e.* have no entropy production, $\langle \Sigma \rangle$ also equals the divergence between the initial and final states of the whole protocol.

If the intermediate process was given by the identity operation $\tilde{\rho}_0 = \mathcal{E}_{\text{id}}(\rho_\tau) = \rho_\tau$, then the entropy production would be $\langle \Sigma_{\text{id}} \rangle = 0$, in agreement with the notion that this process is reversible. On the other hand, if we consider the complete thermalization process, the CPTP map is given by $\tilde{\rho}_0 = \mathcal{E}_{\text{therm}}(\rho_\tau) = \zeta_\beta$, where $\zeta_\beta = \exp(-\beta[H_F(\tau) - F_\beta(\tau)])$ is the Gibbs state at inverse temperature β and with Hamiltonian $H_F(\tau)$, and the equilibrium Helmholtz free energy is $F_\beta(\tau) = -\beta^{-1} \ln(\text{Tr}[\zeta_\beta])$. The entropy production of such intermediate thermalization process becomes $\langle \Sigma_{\text{therm}} \rangle = \Delta S_{\text{therm}} - \beta Q_{\text{therm}}$ [5], where ΔS_{therm} and Q_{therm} are the entropy and energy change of the system during the thermalization. The identity and thermalization processes are somewhat typical thermodynamic processes: either one does nothing, in which case there is no irreversibility, or one lets the system thermalize with a heat reservoir, an ubiquitous process in thermodynamics. Now, we discuss the entropy production of decorrelating processes, capable of erasing classical or quantum correlations even without the presence of heat reservoirs.

We assume in the following that the system is composed by two subsystems, A and B , and the unitary evolution results from their interaction. Let us start considering a local-dephasing process acting on both subsystems, defined by the CPTP map

$$\begin{aligned} \mathcal{E}_{\text{deph}}(\rho^{AB}) &= \sum_{k,l} P_k^A \Pi_l^B \rho^{AB} P_k^A \Pi_l^B \\ &= \sum_{k,l} p(k,l) P_k^A \Pi_{il}^B, \end{aligned} \quad (2)$$

where $\{P_k^A\}$ and $\{\Pi_l^B\}$ are the eigenoperators of the reduced states ρ^A and ρ^B , respectively, and $p(k,l) = \text{Tr}_{AB}[P_k^A \Pi_l^B \rho^{AB}]$. The resulting state of Eq. (2) is a classically-correlated quantum state [28], which means that the local-dephasing process erases all the quantum correlations present in the state ρ^{AB} . Physically, local dephasing can be realized in two ways. Firstly, each subsystem A and B is independently subject to a decoherence process in their eigenbasis. Secondly, a non-selective projective measurement in the eigenbasis of ρ^A and ρ^B is jointly realized, the state in Eq. (2) being the resulting

non-selective state. In the latter situation, $p(k,l)$ is a joint probability of obtaining outcomes k and l for the joint measurement.

Generally, starting from a separable state of the systems A and B , the forward process will create correlations between them, which are quantified by the mutual information $I(\rho^{AB}) = D(\rho^{AB} \parallel \rho^A \otimes \rho^B)$. When the local-dephasing evolution $\mathcal{E}_{\text{deph}}$ is considered as the irreversible intermediate process within the TPM scheme, its resulting entropy production is

$$\begin{aligned} \langle \Sigma_{\text{deph}} \rangle &= D(\rho_\tau^{AB} \parallel \mathcal{E}_{\text{deph}}(\rho_\tau^{AB})) \\ &= S(\mathcal{E}_{\text{deph}}(\rho_\tau^{AB})) - S(\rho_\tau^{AB}). \end{aligned} \quad (3)$$

The last term corresponds to the so-called relative entropy of coherence [29], which is a measure of the quantum correlations present in the state ρ_τ^{AB} [30]. Alternatively, we can write

$$\langle \Sigma_{\text{deph}} \rangle = I(\rho_\tau^{AB}) - I(\mathcal{E}_{\text{deph}}(\rho_\tau^{AB})), \quad (4)$$

illustrating the fact that the effect of the local-dephasing is to erase only the quantum correlations: $I(\rho_\tau^{AB})$ quantifies the total amount of correlations of ρ_τ^{AB} , classical and quantum, while $I(\mathcal{E}_{\text{deph}}(\rho_\tau^{AB}))$ quantifies the total amount of correlations of $\mathcal{E}_{\text{deph}}(\rho_\tau^{AB})$, containing only classical correlations.

In order to connect to the experimental implementation discussed in Sec. V, consider the similar dephasing process in which only system B undergoes the decoherence process,

$$\mathcal{E}_{\text{deph},B}(\rho^{AB}) = \sum_l \Pi_l^B \rho^{AB} \Pi_l^B = \sum_l p(l) \rho_l^A \otimes \Pi_l^B, \quad (5)$$

where

$$\rho_l^A = \frac{\text{Tr}_B[\Pi_l^B \rho^{AB}]}{p(l)} = \sum_k p(k|l) P_{k|l}^A \quad (6)$$

and $P_{k|l}^A$ are the eigenprojectors of state ρ_l^A . If all states ρ_l^A are diagonalized by the same set of projectors $\{P_k^A\}$, the resulting state of Eq. (5) coincides with the resulting state of Eq. (2), with $p(k,l) = p(k|l)p(l)$. In this particular case, we have $\mathcal{E}_{\text{deph},B}(\rho^{AB}) = \mathcal{E}_{\text{deph}}(\rho^{AB})$ meaning that all the quantum correlations of the state ρ^{AB} have been erased by a single dephasing in system B . Therefore, the local dephasing process on system B has the same effect of the local dephasing process for both A and B . In our experimental implementation, we consider only the dephasing in one subsystem.

Let us now consider the complete decorrelating process, where both quantum and classical correlations are fully erased. For an arbitrary state ρ^{AB} , the map describing this process reads $\mathcal{E}_{\text{decor}}(\rho^{AB}) = \rho^A \otimes \rho^B$. This map is generally non-linear, since ρ^{AB} appears inside ρ^A and ρ^B , and therefore it does not correspond to a CPTP map [31] and cannot be realized physically. However,

such a CPTP map can be simulated using simultaneously two copies of the same system and letting interact subsystems of different copies, as will be presented in Sec. V. Assuming its implementation, the resulting entropy production from the TPM scheme gives

$$\langle \Sigma_{\text{decor}} \rangle = I(\rho_{\tau}^{AB}), \quad (7)$$

showing that the entropy production of the complete decorrelating process is precisely given by the information-theoretic cost of erasing all the correlations.

The local thermalization of a bipartite system also comprises a decorrelating process that furthermore involves the typical thermal environment. After the forward process, the system B is coupled to a thermal reservoir that locally thermalizes the system B alone. The CPTP map associated to this process maps the arbitrary bipartite state as $\mathcal{E}_{\text{loc-therm}}(\rho^{AB}) = \rho^A \otimes \zeta_{\beta}^B$, where ρ^A is simply the reduced state of system A while ζ_{β}^B is the Gibbs state reached by system B . During the thermalization of system B , the correlations present in ρ^{AB} are completely erased. Therefore, the resulting entropy production is given by the addition of the complete decorrelation process and the thermalization process,

$$\langle \Sigma_{\text{loc-therm}} \rangle = I_{\tau}^{AB} + D(\rho^B || \zeta_{\beta}^B). \quad (8)$$

In the context of the quantum information processing, deterministic preparation of the system in a given initial state, that is not necessarily thermal from the classical point of view, can also be seen as thermalization with a 'state-preparation' reservoir. In the experimental protocols realized in the present work, the role of local thermalization is played by the reset process bringing one of the subsystems into its initial pure state, see Sec. V.

III. EXPERIMENTAL SYSTEM

One of the simplest systems for studying irreversibility can be composed of a single two-level atom (qubit) interacting with a resonant cavity (harmonic oscillator). This model features quantum properties in a large Hilbert space, while staying relatively simple and providing a good understanding and description of environment interventions. We choose the resonant atom-cavity interaction as a reversible evolution U allowing energy and information exchange within the system, relevant for thermodynamical analysis. Finally, we set the interaction duration to a quarter of the Rabi oscillation period (so-called $\pi/2$ pulse). For the initially excited qubit and the resonator in its ground state, this interaction prepares maximally entangled qubit-resonator states, for which decorrelation effects are the most visible and, thus, easier to detect. In fact, a mutual information between maximally entangled qubit and oscillator reaches its maximal value of 2 bits, insuring a maximal contrasts between correlated and decorrelated states.

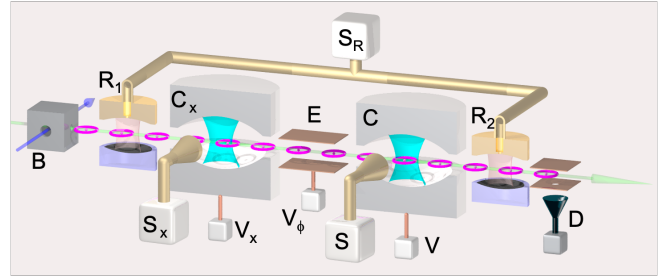


Figure 2. Scheme of the experimental setup. Flying circular Rydberg atoms (toroids), excited in box B, can sequentially interact with two high-quality microwave cavities, C_x and C . The atom-cavity detuning is controlled by electric field applied by voltage potential V_x and V , respectively. The atomic state is manipulated by a low-quality cavity R_1 and is measured by ionization detector M. The cavity state is reconstructed by the Ramsey interferometer (zones R_1 and R_2 fed by source S_R) with a sequence of probe atoms and homodyne microwave field injected by sources S and S_x .

We realize the model qubit-resonator system in a cavity QED setup [14, 21], schematically presented in Fig. 2. Qubits are encoded into circular Rydberg atoms with principle quantum numbers $n = 50$ and 51 . The corresponding levels, denoted by $|g\rangle$ and $|e\rangle$, are separated by 51 GHz. The resonator is a high-quality microwave superconducting cavity C . Its photon lifetime of 65 ms is much larger than the overall experiment duration.

The Rubidium-85 atoms are ejected from an oven, velocity selected by Doppler effect (250 m/s) and excited in box B to the circular Rydberg state $|e\rangle$ by a series of laser, microwave and radio-frequency pulses. The atomic states can be additionally manipulated by classical fields in two Ramsey zones, R_1 and R_2 , fed by a source S_R . The atom-cavity detuning is controlled by an electric field, applied across the metallic resonator's mirrors with potential V , by means of the quadratic Stark effect. In this way we set the exact interaction time and realize the resonant $\pi/2$ interaction. Finally, atomic states are detected by ionisation in a channeltron detector D. The random atom number per atomic sample obeys Poisson statistics. In order to insure a single-atom interaction, we low the mean atom number per sample to about 0.2 atoms and post-select experimental results on detection of exactly one atom.

Our experimental setup consists of two similar cavities, C_x and C , with independent control over atom-cavity interaction. All experiments are performed with cavity C . The auxiliary cavity C_x is used in addition to C in the realization of the complete decorrelation environment and local thermalization, as described later.

We perform full quantum state tomography in order to access quantum state, *i.e.* a complete density matrix, of the joint atom-cavity system. The cavity field is probed by quantum non-demolition (QND) measurement by means of a long sequence of atoms, interacting

dispersively with the cavity field and detected one by one. Being measured in the Ramsey interferometer configuration, composed of two Ramsey cavities, R_1 and R_2 installed before and after C , they provide us information on the photon number distribution in C [32]. The information on the field coherence is extracted by additional homodyne injection of a reference microwave field from source S into C [33]. The atomic states in energy basis are directly detected by ionization in D . An additional $\pi/2$ Rabi pulse applied in zone R_2 before ionization allows for qubit measurement in the x basis of the Bloch sphere. All different measurement settings and the corresponding measurement results from cavity probing and atom detection are combined together in a single MLE algorithm [34] providing us a reconstructed atom-cavity state of the composite system.

IV. QUANTUM STATE RECONSTRUCTION

Estimation of the system's density matrix from an experimental dataset is based on the algorithm presented in Ref. [34]. With sufficiently sensitive measurements and sufficient data, it provides without any particular difficulty the state estimate ρ_{ML} with maximal likelihood of the measured data. Any observable can be directly computed from the set of all measurement results without the need to calculate it from ρ_{ML} . As for other functions of the density matrix, they can be computed from ρ_{ML} . The problem arises for non-linear functions with divergence tendance, like divergence $D(\rho_1||\rho_2)$. If computed between two matrices with different non-full support, the resulting function can be very sensitive to any minor noise in the state reconstruction procedure, making its further use pointless. In the following, we discuss the difficulties of managing the relative entropy for states without full support as well as our method to circumvent this issue.

Estimating the density matrix from experimental dataset: a Bayesian framework

In our experiment, we repeat the preparation-measurement sequence N times for each of the decorrelating processes described above (typically, $N \sim 10^4 - 10^5$). The possible measurement outcomes, labeled as i , are mathematically described by so-called effect matrices E_i [22], which are positive semidefinite matrices, and are such that $\sum_i E_i = 1$. If the system's density matrix is ρ , then outcome i is obtained with probability $p(i|\rho) = \text{Tr}(\rho E_i)$. The key issue is to estimate ρ from the sequence of measurement outcomes $\mathcal{D} = (i_1, \dots, i_N)$. Notice that, as long as the experimental runs are independent from each other, we have $p(\mathcal{D}|\rho) = \prod_{i=1}^N p(i|\rho)$. We adopt here a Bayesian point of view, in which, given the experimental dataset \mathcal{D} , we attribute a likelihood L

to every density matrix using

$$L(\rho|\mathcal{D}) \propto p(\mathcal{D}|\rho). \quad (9)$$

The likelihood function is the basic mathematical object from which physical properties of the system are then estimated, as well as their corresponding uncertainties.

Estimating functions of the density matrix: mean Bayesian estimate

In this work, we focus on estimating non-linear functions of the density matrices, such as the entropy and the KLU divergence between two density matrices. Formally, for a given function $f(\rho)$, we introduce its corresponding likelihood:

$$L_f(x|\mathcal{D}) \equiv \int d\rho L(\rho|\mathcal{D}) \delta(x - f(\rho)), \quad (10)$$

where the integral is over all density matrices (using Haar measure) and δ is the Dirac function. From the L_f function, we may then propose an estimate for $f(\rho)$ given the experimental dataset, as well as its corresponding uncertainty. Here, as an estimate we simply take the average of the L_f distribution:

$$f_{\text{est}} = \langle x \rangle_{L_f} \quad (11)$$

$$= \int dx x L_f(x|\mathcal{D}) \quad (12)$$

$$= \int d\rho f(\rho) L(\rho|\mathcal{D}). \quad (13)$$

Intuitively, every density matrix which is not excluded by the experimental results contributes to the estimate of f , weighted by its corresponding likelihood $L(\rho|\mathcal{D})$.

Similarly, the uncertainty on this estimate is evaluated as the standard deviation of the L_f distribution:

$$\delta f_{\text{est}} = \sqrt{\langle x^2 \rangle_{L_f} - \langle x \rangle_{L_f}^2}. \quad (14)$$

We emphasize that the above-described procedure is not equivalent to the widely-used maximum-likelihood estimate, in which one first introduces the density matrix $\rho_{\text{ML}} = \text{argmax}_{\rho} [L(\rho|\mathcal{D})]$ and then uses $f_{\text{est}} = f(\rho_{\text{ML}})$. While both approaches converge to the same estimate in the limit of infinitely many samples ($N \rightarrow \infty$), they lead to very different results when estimating non-linear functions with a finite number of samples. In particular, it is common that ρ_{ML} is rank-deficient (namely, it has some zero eigenvalues), which leads to nonphysical divergences when estimating the KLU divergence between two density matrices. Furthermore, the approach implemented in this work is conceptually more satisfactory than the MLE reconstruction, as it incorporates the complete statistical information contained in the likelihood function, and is not plagued by the possibly very atypical properties of ρ_{ML} . Notice also that our approach is

conceptually very similar to the so-called mean Bayesian estimate proposed in Ref. [35], where one introduces the density matrix $\rho_{\text{MBE}} = \int d\rho \rho L(\rho|\mathcal{D})$, and then uses $f_{\text{est}} = f(\rho_{\text{MBE}})$. While this is equivalent to our approach when f is a linear function of ρ , our estimate is more generally suited for estimating arbitrary functions of the density matrix.

Sampling density matrices according to their likelihood: Monte-Carlo approach

We limit the cavity's Hilbert space size to 4, allowing thus states with up to 3 photons, reasonable for interactions and protocols realized in this work. Given that density matrices of the atom-cavity system are 8×8 hermitian matrices, one cannot perform directly the integration in a high-dimensional state space as required by Eq. (13) and (14). We circumvent this problem by implementing a numerical Monte-Carlo sampling over density matrices. Concretely, we sample an ensemble of n density matrices (ρ_1, \dots, ρ_n) according to their likelihood, such that $(1/n) \sum_{k=1}^n f(\rho_k) = \int d\rho f(\rho) L(\rho|\mathcal{D}) + O(1/\sqrt{n})$. Namely, averaging over the n sampled density matrices is equivalent to averaging over the L distribution, up to $1/\sqrt{n}$ corrections. This is achieved using the Metropolis algorithm as detailed in Appendix A.

V. SIMULATION OF ENVIRONMENT

In the following, we present the experimental realization of several environments considered in Ref. [5] and discussed in Sec. II. In order to make the environment effect more pronounced, we choose a resonant $\pi/2$ interaction between the atom and the cavity as a unitary forward evolution U_F . The experimental cycle starts with an excited atom in state $|e\rangle$ and the empty cavity in the vacuum state $|0\rangle$, with the corresponding initial joint state

$$\rho_0 = |e0\rangle\langle e0|. \quad (15)$$

The forward evolution U_F transforms ρ_0 into a maximally entangled atom-cavity state

$$\rho_\tau = \frac{1}{2} (|e0\rangle + |g1\rangle) (\langle e0| + \langle g1|). \quad (16)$$

This state exhibits the maximum mutual information I of 2 bits, which is the limit for a two-level subsystem.

To close the cycle, we perform the backward unitary evolution $U_B = U_F^\dagger$. It starts by first applying the σ_x operation on the atomic qubit state and then activating the resonant $\pi/2$ interaction as in U_F . Note that this protocol is similar to the spin-echo technique. Since this cycle must be completed while the atom is crossing the spatial Gaussian mode of the cavity, we realize the first resonant interaction U_F before the atom reaches the center of the

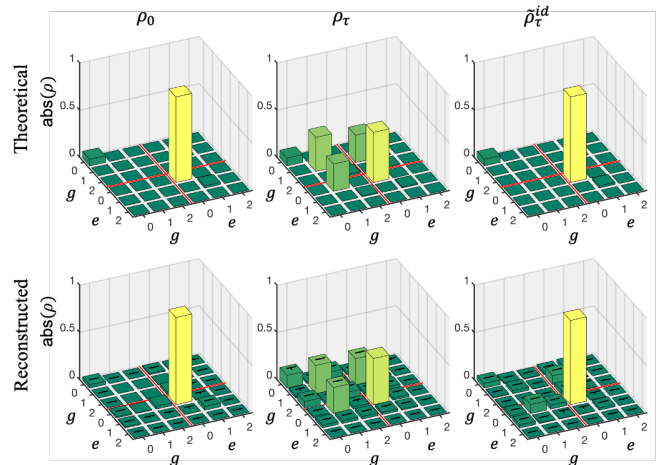


Figure 3. Reconstructed atom-cavity states. Three columns correspond to initial ρ_0 , intermediate entangled ρ_τ and final $\tilde{\rho}_\tau$ states. Upper row: theoretical states based on known experimental imperfections. Lower row: MLE reconstruction. For each atomic state, the cavity photon number is limited by 3 photons. For the sake of clarity, only the absolute values of the density operators are plotted and only up to 2 photons. Red lines on the matrix base delimit the atomic states e and g .

cavity. The σ_x operation is applied when the atom is at the center by detuning it from the cavity resonance by 1 MHz during 0.5 μ s. The exact π spin-flip is calibrated by the Ramsey interferometer [36]. Finally, the second resonant interaction included in U_B is applied while the atom is crossing the second half of the cavity mode.

Figure 3 shows the reconstructed atom-cavity states (absolute values) with the MLE error bars. Here and in the following, theoretical states account for known experimental imperfections. The main effects include finite atomic and photon lifetimes (nonzero population in $|g0\rangle$), dispersion in atom-cavity coupling (reduced coherences $|e0\rangle\langle g1|$), non-ideal σ_x flip (residual coherences in $\tilde{\rho}_\tau^{id}$), and non-negligible presence of a second non-detected atom (populations with double excitation $|e1\rangle$).

No environment action

The first trivial situation we want to observe involves no decorrelation process, *i.e.* no environment coupling. It is equivalent to the forward-backward cycle composed only of U_F and U_B . Ideally, this cycle brings the system back to its initial state, realizing the identity operation:

$$\tilde{\rho}_\tau^{id} = U_F^\dagger U_F \rho_0 U_F^\dagger U_F = \rho_0. \quad (17)$$

The entropy production for this identity process is zero, $\langle \Sigma_{\text{id}} \rangle = D(\tilde{\rho}_\tau^{id} || \rho_0) = 0$.

Figure 4 shows ideal, numerically simulated and experimentally measured entropy production for different

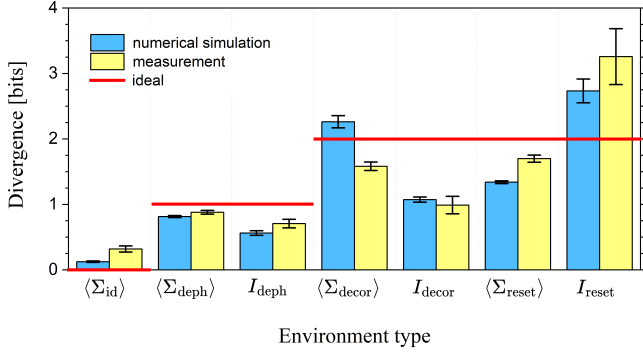


Figure 4. Entropy production for different environments. Simulated results include numerical simulation of both the experimental setup with its known imperfections and the quantum state reconstruction procedure. Red lines indicate the ideal values of 0, 1 and 2 bits of the corresponding environments in the absence of any experimental imperfection and reconstruction noise.

types of environment. Ideal values of information erasure, based on discussion in Sec. II applied to our atom-cavity system interacting resonantly, are indicated by red lines.

For the no-environment case (*i.e.* identity process), both simulated and measured $\langle \Sigma_{\text{id}} \rangle$ are larger than its ideal zero value. Since the divergence D is limited to non-negative values only, any noise in the system's state due to technical imperfections in the state preparation or reconstruction increases the value of the real $\langle \Sigma_{\text{id}} \rangle$. Its value thus quantifies the quality of the realized experimental sequence and its unitary operations, as well as of the MLE protocol.

It is important to note that, here and in the following, all entropic quantities are computed with Monte-Carlo sampling of density matrices, as explained in Sec. IV and Appendix A. If computing these quantities directly from the reconstructed states presented in Figs. 3 and 6, the difference between their ideal, numerically simulated and experimentally measured values is much larger than that seen in Fig. 4 and is more sensitive to experimental uncertainties and MLE parameters. Thus, a significant part of the presented work was dedicated to the development of the more careful data treatment providing more realistic states and their non-linear functions.

Local dephasing

All quantum correlations between two subsystems can be erased by applying local dephasing to one of them. We realize this process by setting large detuning between atomic and cavity frequencies of several MHz for $0.8 \mu\text{s}$, which is done by applying a large electric field V to the atom across C . Since the exact electric field value fluctuates, it induces a random phase shift accumulated between two subsystems, hence dephasing the system.

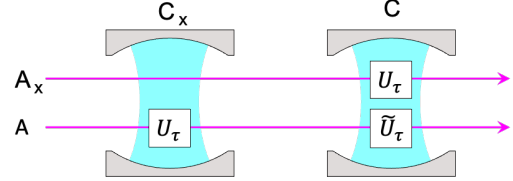


Figure 5. Schematic representation of the complete decorrelation protocol. First, the auxiliary atom A_x interacts with the main cavity C . Next, the main atom A interacts with the auxiliary cavity C_x and then, finally, with the main cavity C .

The efficiency of the phase erasure is verified by applying this detuning in a Ramsey interferometry sequence, where it completely suppresses any contrast on the Ramsey fringes. The ideal dephased state takes the form of a statistical mixture

$$\tilde{\rho}_0^{\text{deph}} = \frac{1}{2} (|e0\rangle\langle e0| + |g1\rangle\langle g1|). \quad (18)$$

The further U_B process does not change this decohered mixture, making $\tilde{\rho}_\tau^{\text{deph}} = \tilde{\rho}_0^{\text{deph}}$.

Figure 6 presents theoretical and reconstructed states $\tilde{\rho}_0$ and $\tilde{\rho}_\tau$ for this process. The corresponding $\langle \Sigma_{\text{deph}} \rangle$ together with the change of the mutual information I_{deph} from ρ_τ and $\tilde{\rho}_0$ is plotted in Fig. 4. They are both lower than their common maximal value of 2 bits due to experimental imperfections. Possibly, the smaller value of I_{deph} compared to $\langle \Sigma_{\text{deph}} \rangle$ results from some systematic uncertainty in the atom-cavity interaction that is partially compensated in the forward-backward cycle (similarly to the spin-echo technique), used to access $\langle \Sigma_{\text{deph}} \rangle$.

Complete decorrelation

Since there exists no CPTP map that implements the complete decorrelation process for an arbitrary state, we experimentally simulate this process employing two atoms (A and A_x) and two cavities (C and C_x), as depicted in Figure 5. The auxiliary atom A_x is sent through the cavities before the main atom A . The atoms go through the auxiliary cavity C_x before entering the main cavity C . We can switch on and off the interactions between any atom and any cavity by detuning the atom with the corresponding Stark electric field, V or V_x , see Fig. 2.

The implemented experimental sequence looks as follows. The auxiliary atom A_x interacts and gets entangled only with the main cavity C , creating the joint state $\rho_{\tau}^{A_x C}$ given by (16). Next, the main atom A gets entangled with the auxiliary cavity C_x , creating a similar state $\rho_{\tau}^{A C_x}$ of the $A-C_x$ system. In this part of the sequence, the atoms and the cavities are in the same reduced state $\rho_{\tau}^{A_x} = \rho_{\tau}^A$ and $\rho_{\tau}^{C_x} = \rho_{\tau}^C$, respectively. Therefore, when the main atom enters the main cavity, their joint state is $\tilde{\rho}_0^{\text{decor}} = \rho_{\tau}^A \otimes \rho_{\tau}^C$. This state corresponds to the state ρ_{τ}

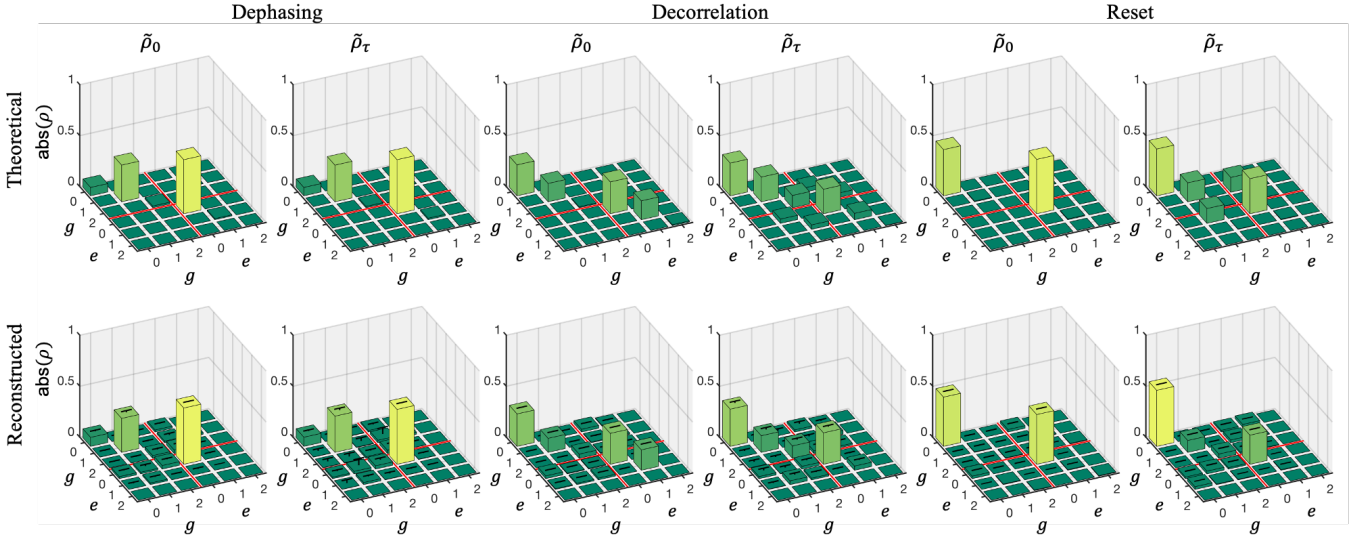


Figure 6. Reconstructed atom-cavity states for three types of decorrelating processes: dephasing, complete decorrelation and reset to initial state. Upper and lower rows are theoretical and experimentally reconstructed density matrices.

followed by the complete decorrelation process. Ideally, it reads

$$\tilde{\rho}_0^{decor} = \frac{1}{4} (|e\rangle\langle e| + |g\rangle\langle g|) \otimes (|0\rangle\langle 0| + |1\rangle\langle 1|). \quad (19)$$

The backward process closing the cycle is implemented by the U_B between A and C. The system's state at the end of the cycle then reads

$$\tilde{\rho}_\tau^{decor} = \frac{1}{4} (|g0\rangle\langle g0| + |g1\rangle\langle g1| + |e0\rangle\langle e0| + |\psi_2\rangle\langle\psi_2|), \quad (20)$$

with the double-excitation contribution $|\psi_2\rangle = \cos(\theta)|e1\rangle + \sin(\theta)|g2\rangle$ and $\theta = \sqrt{2\pi}/4$.

The entropy production $\langle \Sigma_{decor} \rangle$ of this process, erasing all correlations in the system, ideally reaches its maximum possible value of 2 bits. However, the measured values of $\langle \Sigma_{decor} \rangle$ and I_{decor} are significantly less than this level. This difference comes from higher sensitivity of the current experimental sequence of the setup imperfections when using different quantum systems to mimic the same one. In such a way, any dispersion in their properties, like exact position of the atoms inside the cavities, will unbalance the forward and backward parts of the cycle, realized with different atoms and cavities. This might also qualitatively explain why the numerically simulated and measured values of I_{decor} are closer to each other than the corresponding values of $\langle \Sigma_{decor} \rangle$, extracted from a longer experimental sequence.

Local thermalization

The local thermalization process in the considered model system requires resetting one of the subsystems back to its initial state. Realizing this reset in a short

time interval between U_F and U_B either on the atom or on the cavity is nontrivial and challenging. It demands sophisticated modification of the atom-cavity interaction sequence and inclusion of auxiliary atoms and/or microwave pulses.

If we choose to reset the cavity state, a similar evolution can be realized by making the atom to interact with two cavities, C_x and C, prepared in the same initial vacuum state $|0\rangle$. First, we let the atom to perform the forward evolution U_F in C_x . The state of the A-C system, after tracing out the state of C_x , reads

$$\tilde{\rho}_0^{reset} = \frac{1}{2} (|g\rangle\langle g| + |e\rangle\langle e|) \otimes |0\rangle\langle 0|, \quad (21)$$

effectively resetting the cavity back to its initial vacuum state. The cycle is closed by the backward process U_B between A and C, similarly to all previous protocols. Note that this experimental scheme is identical to the one of complete decorrelation, see Fig. 5, but without auxiliary atom A_x . The state reconstruction is finally performed on the A-C system. Ideally, the system comes to the state

$$\tilde{\rho}_\tau^{reset} = \frac{1}{2} |g0\rangle\langle g0| + \frac{1}{2} (|e0\rangle + |g1\rangle)(\langle e0| + \langle g1|). \quad (22)$$

For the sake of simplicity, the reset process has been realized by the same experimental sequences programmed to simulate complete decorrelation with two atoms and two cavities, see Fig. 5. Since atomic samples have random number of real atoms, the decorrelation process was implemented by experimental sequences conditioned on the final detection of both atoms, A_x and A. For the reset environment, on the contrary, we have post-selected sequences conditioned on the successful detection of only one atom A and with no atoms in the sample A_x .

As in the case of complete decorrelation, the reset process completely erases 2 bits of information stored in ρ_τ ,

although in a different way. Figure 4 shows the values of both $\langle \Sigma_{\text{reset}} \rangle$ and I_{reset} . Numerically simulated and experimentally measured values are reasonably close, demonstrating our good understanding of the system’s main characteristics. At the same time, similarly to the decorrelation protocol, the use of different atoms to simulate a single qubit leads to a significant difference between $\langle \Sigma_{\text{reset}} \rangle$ and I_{reset} .

VI. CONCLUSIONS

We have simulated several basic types of non-thermal environment [5] that erase different information and correlation in a bipartite quantum system. As a model system, we have manipulated single circular Rydberg atoms interacting resonantly with a high-finesse cavity mode. Following the two-point measurement approach, the experimental sequences are composed of three basic processes: unitary forward evolution, interaction with environment and backward unitary evolution. The irreversibility of thermodynamical cycles containing unitary (atom-cavity interaction) and non-unitary (coupling to environment) evolution is quantified by the entropy production $\langle \Sigma \rangle$, computed as the Kullback-Leibler-Umegaki divergence between the initial and final states of the system. All these states are estimated by full quantum state tomography based on quantum non-demolition measurement of the photon number in the cavity and the state-selective atom detection.

After our initial data analysis, we encountered an unforeseen difficulty when computing entropic quantities from reconstructed density matrices. Being close to pure states (a frequent occurrence for quantum information systems) and being rank-deficient (the feature of the maximum-likelihood estimation), reconstructed density operators can lead to excessively strong divergent behavior of the entropy production $\langle \Sigma \rangle$. As the name suggests, the KLU divergence D does diverge for states with different support. Being used to quantify the entropy production, this property of D reflects the third law of thermodynamics prohibiting zero-entropy states, like *e.g.* thermal state with zero temperature, whose preparation would require infinite entropy production. For any other classical thermal state, the density operators are always full-rank, thus resulting in finite D . On the contrary, for quantum systems in or close to pure states, like qubits in quantum superposition states, the divergence fails to adequately describe the system’s evolution and its irreversibility. This fact should not surprise us, as the classical third law strictly prohibits zero-entropy states and thus the diverging entropy production defined as the KLU divergence, that is perfectly adapted to the classical realm, starts to fail at quantum level.

Although we have managed to partially overcome the problem of the divergence for experimental MLE states, the general question remains relevant: how adequate is the widespread use of this quantity to characterize any

thermodynamical processes in quantum systems? Or should we look for a replacement that would allow us to more accurately quantify irreversibility at the quantum level with less dependence on measurement accuracy and a particular state reconstruction algorithm? We hope that this work will draw the attention of the community to this problem of quantum thermodynamics.

VII. ACKNOWLEDGMENTS

This work was supported by the Foundational Questions Institute Fund (Grant number FQXi-IAF19-05), the Templeton World Charity Foundation, Inc (Grant No. TWCF0338), ANR Research Collaborative Project “Qu-DICE” (ANR-PRC-CES47) and ANR Single-team Research Project “ProRydAQS” (ANR-24-CE47-2923-01).

Appendix A: Monte-Carlo sampling of density matrices according to their likelihood

The numerical approach to sample density matrices according to their likelihood is achieved using a standard Metropolis algorithm. First, we initialize the algorithm to an arbitrary density matrix ρ_0 (in practice, we start with ρ_{ML}). We then construct a Markov chain by iterating the following steps:

- propose a new density matrix ρ_{new} ;
- if $L(\rho_{\text{new}}) > L(\rho_k)$, then accept the move;
- otherwise, accept the move with probability $L(\rho_{\text{new}})/L(\rho_k)$;
- if the move is accepted, then $\rho_{k+1} = \rho_{\text{new}}$;
- otherwise, keep $\rho_{k+1} = \rho_k$.

Here, the index k labels iteration loops.

A sufficient condition for convergence of the Markov chain towards the $L(\rho)$ distribution is that of detailed balance, which is guaranteed if the probability to propose the move to ρ_{new} starting from ρ_k is the same as the probability to propose the move to ρ_k starting from ρ_{new} . This is ensured in our algorithm by proposing moves of the form $\rho_{\text{new}} = \rho_k + \epsilon - \text{Tr}(\epsilon) \frac{1}{d}$, where ϵ is a $d \times d$ hermitian matrix whose coefficients are all independently drawn from a Gaussian distribution of zero mean and standard deviation σ . The Hilbert space dimension is $d = 8$ to which we truncate our experimental analysis. Whenever ρ_{new} happens to have negative eigenvalues, the move is always rejected (namely, ρ_{new} has a vanishing likelihood). The standard deviation σ is automatically adjusted throughout the sampling procedure so that the mean acceptance rate of the proposed moves remains between 0.4 and 0.6. Finally, in order to obtain samples with a good statistical independence, between each collected density matrix we run about 10^5 individual Metropolis steps as described above, and collect in this way an ensemble of $n = 100$ density matrices for each decorrelation scenario.

[1] M. W. Zemansky and R. H. Dittman, *Heat and thermodynamics* (The McGraw-Hill Companies, Inc., 1997).

[2] M. Esposito, K. Lindenberg, and C. Van den Broeck, Entropy production as correlation between system and reservoir, *New Journal of Physics* **12**, 013013 (2010).

[3] T. Sagawa and M. Ueda, Role of mutual information in entropy production under information exchanges, *New Journal of Physics* **15**, 125012 (2013).

[4] J. M. R. Parrondo, J. M. Horowitz, and T. Sagawa, Thermodynamics of information, *Nature Physics* **11**, 131 (2015).

[5] G. T. Landi and M. Paternostro, Irreversible entropy production: From classical to quantum, *Rev. Mod. Phys.* **93**, 035008 (2021).

[6] J. Goold, M. Huber, A. Riera, L. d. Rio, and P. Skrzypczyk, The role of quantum information in thermodynamics - a topical review, *Journal of Physics A: Mathematical and Theoretical* **49**, 143001 (2016).

[7] R. Kosloff, Quantum thermodynamics: A dynamical viewpoint, *Entropy* **15**, 2100 (2013).

[8] H. Tasaki, *Jarzynski relations for quantum systems and some applications* (2000), arXiv:cond-mat/0009244 [cond-mat.stat-mech].

[9] S. Suomela, P. Solinas, J. P. Pekola, J. Ankerhold, and T. Ala-Nissila, Moments of work in the two-point measurement protocol for a driven open quantum system, *Phys. Rev. B* **90**, 094304 (2014).

[10] S. Kullback and R. A. Leibler, On Information and Sufficiency, *The Annals of Mathematical Statistics* **22**, 79 (1951).

[11] H. Umegaki, Conditional expectation in an operator algebra, I, *Tohoku Mathematical Journal* **6**, 177 (1954).

[12] T. B. Batalhão, A. M. Souza, R. S. Sarthour, I. S. Oliveira, M. Paternostro, E. Lutz, and R. M. Serra, Irreversibility and the arrow of time in a quenched quantum system, *Phys. Rev. Lett.* **115**, 190601 (2015).

[13] P. A. Camati, J. P. S. Peterson, T. B. Batalhão, K. Micodei, A. M. Souza, R. S. Sarthour, I. S. Oliveira, and R. M. Serra, Experimental rectification of entropy production by maxwell's demon in a quantum system, *Phys. Rev. Lett.* **117**, 240502 (2016).

[14] B.-L. Najera-Santos, P. A. Camati, V. Métillon, M. Brune, J.-M. Raimond, A. Auffèves, and I. Dotsenko, Autonomous Maxwell's demon in a cavity QED system, *Phys. Rev. Research* **2**, 032025 (2020).

[15] L. Mancino, M. Sbroscia, E. Roccia, I. Gianani, F. Somma, P. Mataloni, M. Paternostro, and M. Barbieri, The entropic cost of quantum generalized measurements, *npj Quantum Information* **4**, 20 (2018).

[16] P. M. Harrington, D. Tan, M. Naghiloo, and K. W. Murch, Characterizing a statistical arrow of time in quantum measurement dynamics, *Phys. Rev. Lett.* **123**, 020502 (2019).

[17] M. Rossi, L. Mancino, G. T. Landi, M. Paternostro, A. Schliesser, and A. Belenchia, Experimental assessment of entropy production in a continuously measured mechanical resonator, *Phys. Rev. Lett.* **125**, 080601 (2020).

[18] G. Adesso, T. R. Bromley, and M. Cianciaruso, Measures and applications of quantum correlations, *Journal of Physics A: Mathematical and Theoretical* **49**, 473001 (2016).

[19] A. Galindo and M. A. Martín-Delgado, Information and computation: Classical and quantum aspects, *Rev. Mod. Phys.* **74**, 347 (2002).

[20] N. Gisin, G. Ribordy, W. Tittel, and H. Zbinden, Quantum cryptography, *Rev. Mod. Phys.* **74**, 145 (2002).

[21] S. Haroche, Nobel lecture: Controlling photons in a box and exploring the quantum to classical boundary, *Rev. Mod. Phys.* **85**, 1083 (2013).

[22] P. Six, P. Campagne-Ibarcq, I. Dotsenko, A. Sarlette, B. Huard, and P. Rouchon, Quantum state tomography with noninstantaneous measurements, imperfections, and decoherence, *Phys. Rev. A* **93**, 012109 (2016).

[23] G. Manzano, J. M. Horowitz, and J. M. R. Parrondo, Quantum fluctuation theorems for arbitrary environments: Adiabatic and nonadiabatic entropy production, *Phys. Rev. X* **8**, 031037 (2018).

[24] Y. Morikuni and H. Tasaki, Quantum jarzynski-sagawa-ueda relations, *Journal of Statistical Physics* **143**, 1 (2011).

[25] M. Campisi, P. Hänggi, and P. Talkner, Colloquium: Quantum fluctuation relations: Foundations and applications, *Rev. Mod. Phys.* **83**, 771 (2011).

[26] Y. Murashita, Z. Gong, Y. Ashida, and M. Ueda, Fluctuation theorems in feedback-controlled open quantum systems: Quantum coherence and absolute irreversibility, *Phys. Rev. A* **96**, 043840 (2017).

[27] P. A. Camati and R. M. Serra, Verifying detailed fluctuation relations for discrete feedback-controlled quantum dynamics, *Phys. Rev. A* **97**, 042127 (2018).

[28] G. Bellomo, A. Majtey, A. Plastino, and A. Plastino, Quantum correlations from classically correlated states, *Physica A: Statistical Mechanics and its Applications* **405**, 260 (2014).

[29] T. Baumgratz, M. Cramer, and M. B. Plenio, Quantifying coherence, *Phys. Rev. Lett.* **113**, 140401 (2014).

[30] S. Luo, Using measurement-induced disturbance to characterize correlations as classical or quantum, *Phys. Rev. A* **77**, 022301 (2008).

[31] D. R. Terno, Nonlinear operations in quantum-information theory, *Phys. Rev. A* **59**, 3320 (1999).

[32] C. Guerlin, J. Bernu, S. Deléglise, C. Sayrin, S. Gleyzes, S. Kuhr, M. Brune, J.-M. Raimond, and S. Haroche, Progressive field-state collapse and quantum non-demolition photon counting, *Nature* **448**, 889 (2007).

[33] S. Deléglise, I. Dotsenko, C. Sayrin, J. Bernu, M. Brune, J.-M. Raimond, and S. Haroche, Reconstruction of non-classical cavity field states with snapshots of their decoherence, *Nature* **455**, 510 (2008).

[34] V. Métillon, S. Gerlich, M. Brune, J. M. Raimond, P. Rouchon, and I. Dotsenko, Benchmarking maximum-likelihood state estimation with an entangled two-cavity state, *Phys. Rev. Lett.* **123**, 060404 (2019).

[35] R. Blume-Kohout, Optimal, reliable estimation of quantum states, *New Journal of Physics* **12**, 043034 (2010).

[36] M. Penasa, S. Gerlich, T. Rybarczyk, V. Métillon, M. Brune, J. M. Raimond, S. Haroche, L. Davidovich, and I. Dotsenko, Measurement of a microwave field amplitude beyond the standard quantum limit, *Phys. Rev. A* **94**, 022313 (2016).